https://erjm.journals.ekb.eg
ISSN: 1110-1180

DOI: 10.21608/erjm.2021.46710.1047

ERJ
Engineering Research Journal
Faculty of Engineering
Menoufia University

Experimental and CFD Study on Single Slope Double Basin Solar Still

Mahmoud S. El-Sebaey[1]*, Ahmed Hegazy[1], Asko Ellman[2] and Tarek Ghonim[1]

[1]Mechanical Power Engineering Department, Faculty of Engineering
Menoufia University, Sheben El-Kom, Egypt

[2] Faculty of Engineering and Natural Sciences, Tampere University, Finland

** Corresponding author: eng_mahmoudelsebaey@yahoo.com*

ABSTRACT

The shortage of drinkable water in many areas of the world represents a fatal problem. The desalination of saltwater can be a solution to this problem. Solar still was a simple and reliable system to be used in arid and sunny regions, but it has the disadvantage of relatively low productivity. A new configuration of solar still, namely single slope double basin solar still, was proposed in the current work to increase productivity. A prototype of this still type was designed, fabricated, and tested. Besides, a multi-phase, three-dimensional CFD model for mass and heat transfer under unsteady conditions of such still type using CFD ANSYS was developed. This model enabled predicting the performance of this still configuration. The simulation results were validated with experimental data for the climate conditions of Sheben El-Kom, Egypt (latitude 30.5° N and longitude 31.01° E). Within the scope of this study, simulation results were found to be in good agreement with the experimental data. The daily simulated and experimental accumulated productivities of the single slope double basin solar still were found to be 3.148 lit/m^2 and 2.855 lit/m^2 for a water-/equivalent water depth of 2cm. Also, the simulated and experimental daily efficiencies were around 27.65% and 25%, respectively for the tested water-/ equivalent water depth, whereas the reported highest efficiency of the conventional single-slope single basin solar still was 15.5%.

Keywords: *Single Slope; double Basin; Solar Still; CFD ANSYS; Thermal Desalination; Egyptian Climate.*

1. Introduction

Many people feel that they were entitled to limitless quantities of drinkable freshwater. Unfortunately, there were a distinct number of water stress areas on Earth. According to UNICEF, globally, more than 1.1 billion people do not have potable water and about 1000 children, under the age of five, die daily because of diseases coming from undrinkable water. Lack of freshwater can even affect war conflicts, especially in water-stressed areas, [1].

There were various high and medium technologies available for water desalination; viz. Multi Stage Flash (MSF) desalination, Multiple Effect Distillation (MED) [2], Thermal Vapor Compression (TVC) [3], Membrane Distillation (MD) [4], Reverse Osmosis (RO) [5] and others. All these technologies depend on conventional source of energy (electricity) and require high-tech parts i.e. batteries, filters or membranes, etc. The basin type solar still was the simplest, cost-effective, and environmentally-friendly technology for water purification [6]. However, this still type suffers relatively low productivity. Several investigations have been carried out to study new configurations of the basin type solar still aiming at enhancing its productivity; these investigations have been described in detail in Ref. [7]. One of these investigations was studying experimentally double slope, double basin, solar still [8]. The researchers in [8] concluded that double basin insulated and un-insulated stills gave 17.38% and 8.12% higher production than the single basin still for 1 cm water depth.

It was stated in [9] that for sites with latitude higher than 20^o, a single slope was more practical than double slope solar still. Also, in the latter still, a considerable part of the still basin was shaded by the holders of the transparent covers and part of the incident solar radiation can penetrate the covers to the outside where less solar radiation reaches the basin base. Besides, the average incident angle of the falling radiation on the still covers was relatively high which results in reducing the transmissivity of the covers, and thus the absorption of the base of the

still basin for solar radiation was reduced. As a result of this explanation a new configuration of the basin solar still was proposed in [10], namely single slope double basin solar still SSDBSS. It was shown analytically and experimentally in [10] that this still was more efficient and advantageous than already existing solar still configurations. This was due to the influence of dividing the saltwater into two basins and shrinkage of the air gaps volume of the SSDBSS.

A few researchers have developed CFD models of a simple conventional basin type solar still and use it for performance enhancement by some parametric analysis, [11-18]. Setoodeh et al. [19] developed a multiphase simulation model for heat and mass transfer and carried out experiments for the conventional single slope solar still. They concluded that the water temperatures predicted by CFD were in acceptably good agreement with the experimental results.

For the optimal choice of the dimensions, thermal and optical parameters of the SSDBSS to operate under specific conditions, it was very laborious and expensive to carry out this task experimentally. As a result, an effectual tool for simulating heat and mass transfer inside the still, was necessary that can lead to predicting the still performance under the given operating circumstances. For this purpose, a 3-D CFD model was developed with aid of ANSYS FLUENT for simulating the heat and mass transfer inside the SSDBSS. Therefore the present research aimed to develop a 3-dimensional, multi phase CFD model of single slope double basin solar still SSDBSS to understand the evaporation and condensation phenomena in solar still. The model will be developed with the help of ANSYS FLUENT R15.0 Workbench. Besides, the fabrication and performance evaluation of single slope, double basin solar still design was presented. The simulation results were compared with experimental data. Water and glass cover temperatures and yield of freshwater from the simulation results compared with the experimental results.

2. Experimental Setup

To be able to validate the developed simulation model for the SSDBSS a prototype of the proposed solar still configuration was designed, fabricated, and tested. Figures 1 and 2 depict a schematic drawing and a photograph of the fabricated SSDBSS, respectively. The still consists of two airtight basins; the lower basin was made of a galvanized iron sheet of 0.8 mm thickness with a dimension of 1000mm x 1000mm and it contains saltwater. The upper basin made of a 4 mm thickness acrylic sheet, was fixed on the side edges of the lower basin. The inner height of the frontal vertical side of the still was kept at 100 mm. Window glass of 3 mm thickness was used as the transparent cover of the upper basin with 23° inclination at the top of the still. The inner bottom of the lower basin was black coated to improve radiation absorption. The upper basin was left uncoated to maintain its transparency and allow the incident solar radiation to penetrate to the lower part of the still. The other interior faces (back, front, and two sidewalls) of the still were painted with white paint to enhance radiation reflectivity. Ten equally spaced vertical acrylic strips of 50 mm height and 3 mm thickness were fitted to the cavity of the upper part parallel to the frontal and rear walls. They were fixed to the base of the cavity and sidewalls using adhesive silicone rubber glue, and they form ten compartments that serve to hold saltwater. The top glass window cover and the upper basin can easily be assembled and reassembled, which eases cleaning and black coating. The outer frame of the still was made of 10 mm thickness wood sheets. Mounted on this frame, an insulating layer of 50 mm thickness made of wood chips was used to reduce the heat loss from the still to the outlet. Ten tubes with 10 mm diameter were inserted through holes in one side of both sides of the wooden box and upper still body of the SSDBSS, and they were fixed to the inner surface, using adhesive silicone rubber glue at a distance of 40 mm from the lower edge of each compartment. These tubes were fitted with valves for allowing saltwater to flow into the compartments of the upper still internal body part and prevent the air to stream outside this still part. Similar ten tubes were fitted to the other sidewall, but at the lowest position of each compartment for draining the brine.

Two channels were fitted internally to the frontal still side just below the transparent covers of the still to collect the distillate. They were 10^{o} tilted toward the outlet tubes that were provided to drain and store the condensate in measuring jars. Provisions to supply saline water and to drain the basin water were made. Calibrated Thermocouple insertions [Chromel-Alumel (Type-K)] were also made to read the temperatures. The experimental setup was arranged in a way to face the south direction to receive the maximum solar radiation. A silicon rubber sealant was used to seal the glass cover and acrylic basin with the body of the still, to prevent leakage of the evaporated vapor. The basins of the still were cleaned frequently to avoid the deposition of salts and foreign particles.

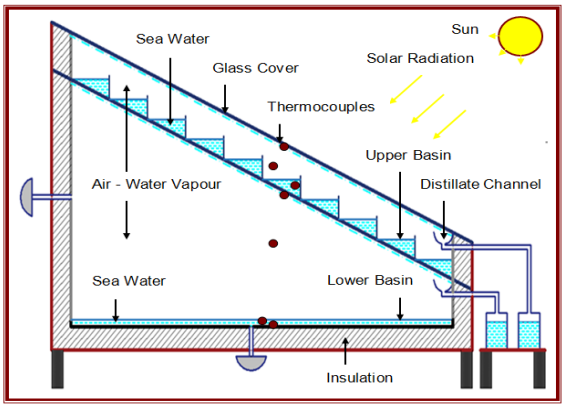

Fig. 1: Illustrative figure of the single slope double basin solar still.

Fig. 2: A photograph of the single slope double basin solar still.

3. CFD Modeling:

3.1. Geometry Creation and Meshing Details

The first step in CFD analysis of any problem was the creation of the geometric model of the problem domain as per the design specifications. The domain considered here, was the two cavities above the water surfaces of the still basins and confined by the still sides above these surfaces and the acrylic base and the glass cover of the upper basin. A 3-D geometry of the SSDBSS was created by ANSYS Workbench which provides a Design Modeler as a design tool to develop the geometric models of the physical problem domain. Figure 3 shows the geometric model of the SSDBSS with the same dimensions of the designed experimental model, which was imported to the ANSYS meshing module.

Since the geometry of the SSDBSS does not involve any type of curved surfaces so the CutCell method of meshing was most suited and can provide accurate results with moderate computation time required by using ANSYS workbench MESHING as shown in Fig. 4. The total numbers of nodes and elements in the meshed domain were 1320947and 1226770, respectively, which were enough for the complexity of the problem at hand.

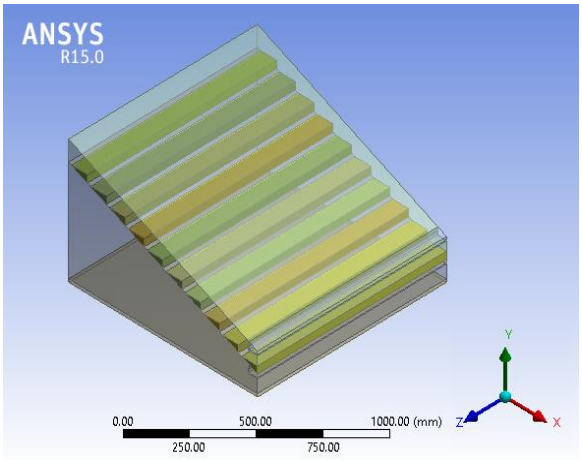

Fig. 3: Geometric model of the single slope, double basin solar still.

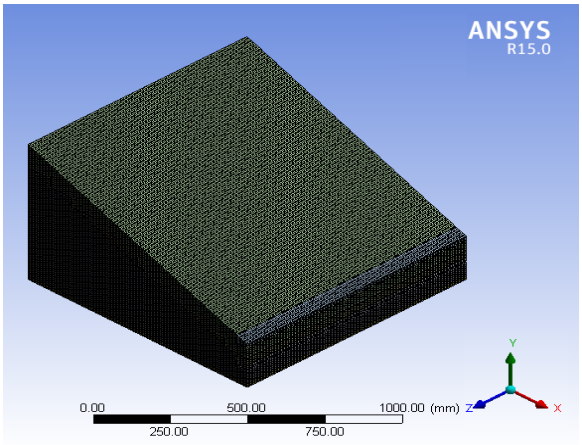

Fig. 4: Meshed CFD domain the single slope, double basin solar still.

Having generated the mesh, it was important to check its quality since it can affect the accuracy of the solution to a great extent. There were several parameters available with ANSYS Workbench for checking the quality of the mesh. Some of these important parameters were Element Quality, Skewness, Aspect Ratio and Orthogonal Quality, etc. In this study, these parameters have been checked. In a good meshed domain there has to be a very little or negligible number of elements having the Skewness value equal to 1. An element having a Skewness value of 1 was in general considered to be an unviable element. From the survey, the average value of Skewness should always be less than 0.3 for a good quality mesh. Fig. 5 shows that most of the elements have Skewness values less than 0.13.

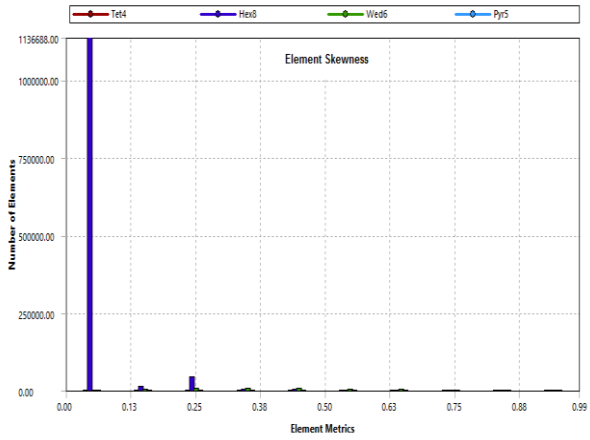

Fig. 5: Skewness of the elements of the single slope, double basin solar still.

Similarly, the Aspect Ratio was also a parameter for the assessment of the quality of a generated mesh. For 3-D elements, the Aspect Ratio was a measure of the stretching of a cell, and it was defined as the ratio of the maximum value to the minimum one of any of the following distances: the normal distances between the cell centroid and face centroids, and the distances between the cell centroid and nodes. The average value of the Aspect Ratio for a good quality mesh should be less than 2. Figure 6 shows, that most of the elements were having a value of aspect ratio less than 2. This indicates that generated mesh that has mostly hexahedron elements was a good quality mesh for the Skewness as well as Aspect Ratio.

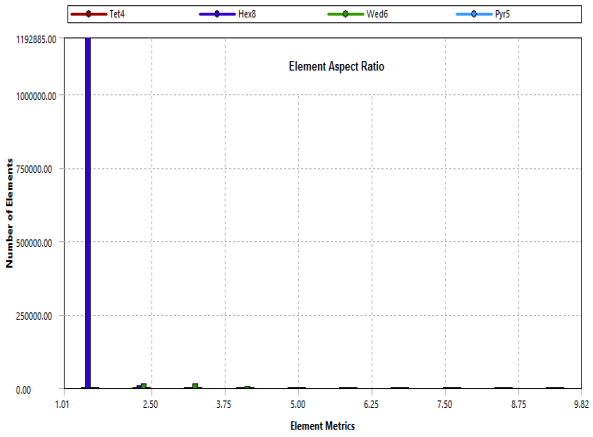

Fig. 6: Aspect Ratio of the elements of the single slope, double basin solar still.

3.2. Assumptions for Simulation

The following assumptions were considered here for the CFD simulation modeling:

1. There was no internal source of thermal-energy generation.

2. As the ambient wind velocity was low, the effect of wind velocity was neglected and only free convection was taken into account.

3. Only film type condensation comes about in place of drop type condensation.

4. No leakages occur in the system.

5. The physical bottom and sidewalls of the system were insulated and hence they were considered adiabatic.

6. The water level was kept constant inside the basin and energy transfer by inlet and outlet liquid masses were negligible.

7. As variation in temperatures was low, properties of the fluids such as specific heat, thermal conductivity, viscosity, and density were taken as a piecewise-linear profile with temperature while the physical properties of the walls were taken as constant.

8. There was no temperature gradient across the basins water and the transparent covers of the solar still.

9. The acrylic base of the upper basin was considered to have neglected thermal capacity.

3.3. Governing Equations

Solar radiation with intensity G falls on the glass cover of the SSDBSS. Thermal power $(1-\tau_{gu})$ G A_b penetrates the glass cover and $(1-\tau_{gu})$ α_{wu} G A_b was absorbed by the saltwater contained in the upper basin. The thermal power $(1-\tau_{gu})$ $(1-\alpha_{wu})$ $(1-\tau_{acu})$ G A_b goes through the water in the upper basin to the lower basin. The thermal power $(1-\tau_{gu})$ $(1-\alpha_{wu})$ $(1-\tau_{acu})$ α_b G A_b was absorbed by the base of the lower basin along with the saltwater held in it. Most of the thermal power absorbed by the lower and upper basin causes temperature rises in saltwater, which leads to increasing the temperatures of the air above them and giving rise to the air to be saturated. The hot wet air goes up and touches the cooler transparent covers (acrylic base of the upper basin and the glass cover) and gets cooled. Hence, some of the moisture content in the air was condensed and the condensate droplets slide on the inner surfaces of the transparent covers to the collecting channels and go out to the collecting jars. Thermal power rates $\dot{q}_{rl}$, $\dot{q}_{cl}$ and $\dot{q}_{evl}$ by radiation, convection, and evaporation,

respectively, were transferred from the water surface in the lower basin to the acrylic base of the upper basin. These heat rates were absorbed by the upper basin base which in turn transfers them to the saltwater in the upper basin since the base was assumed to have neglected thermal capacity. Accordingly, an unsteady condition heat balance for the water mass m_l of the lower basin can be given by:

$$(1-\tau_{gu})(1-\alpha_{wu})(1-\tau_{acu})\,\alpha_b G A_b = \dot{q}_{rl}+\dot{q}_{cl}+\dot{q}_{evl}+m_l c_w \frac{\partial T_l}{\partial t}$$

(1)

Likewise thermal power rates $\dot{q}_{ru}$, $\dot{q}_{cu}$ and $\dot{q}_{evu}$ by radiation, convection, and evaporation, respectively, were transferred from the water surface in the upper basin to the glass of the upper basin. Hence, an unsteady heat balance for the upper basin can be obtained as:

$$\dot{q}_{rl}+\dot{q}_{cl}+\dot{q}_{evl}+(1-\tau_{gu})\,\alpha_{wu} G A_b = \dot{q}_{ru}+\dot{q}_{cu}+\dot{q}_{evu}+m_u c_w \frac{\partial T_u}{\partial t}$$

(2)

An unsteady thermal balance for the glass cover of the upper basin leads to obtain the following equation:

$$\dot{q}_{ru}+\dot{q}_{cu}+\dot{q}_{evu}+G A_b \alpha_{gu} = \dot{q}_{rg}+\dot{q}_{cg}+m_g c_g \frac{\partial T_g}{\partial t}$$

(3)

$\dot{q}_{rl}$, $\dot{q}_{cl}$, $\dot{q}_{evl}$, $\dot{q}_{ru}$, $\dot{q}_{cu}$, $\dot{q}_{evu}$, $\dot{q}_{rg}$, and $\dot{q}_{cg}$ can be determined as described briefly in Refs. [20 and 21].

Beside the above mentioned equation, the differential equations describing flow, heat and mass transfer of the wet air inside the cavities of the studied domain for the unsteady state condition and used in the developed CFD models were based on the continuity, momentum and energy transfer conservation principles.

Energy Equation

The energy equation for the mixture was given below [22]:

$$\frac{\partial}{\partial t}\sum_{k=1}^{n}\left(\alpha_k \rho_k E_k + \nabla.\sum_{k=1}^{n}\left(\alpha_k \bar{v}_k (\rho_k E_k + P)\right)\right) = \nabla.\left(K_{eff}\nabla T\right)+S_E$$

(4)

Where K_{eff} was the effective conductivity.

Continuity equation

The continuity equation for the mixture was [22]:

$$\frac{\partial}{\partial t}(\rho_m)+\nabla.\left(\rho_m \bar{v}_m\right)=0$$

(5)

Where $\bar{v}_m$ was the mass-averaged velocity:

$$\bar{v}_m = \frac{\sum_{k=1}^{n}\alpha_k \rho_k \bar{v}_k}{\rho_m}$$

(6)

Momentum equation

The momentum equation for the mixture can be attained by adding each momentum equation for all the phases. It can be expressed as [22]:

$$\frac{\partial}{\partial t}\left(\rho_m \bar{v}_m\right)+\nabla.\left(\rho_m \bar{v}_m x \bar{v}_m\right) = -\nabla p+\nabla.\left[\mu_m\left(\nabla \bar{v}_m+\nabla \bar{v}_m^{\,T}\right)\right]+\rho_m \bar{g}+\bar{F}+\nabla.\left(\sum_{k=1}^{n}\alpha_k \rho_k \bar{v}_{dr,k} x \bar{v}_{dr,k}\right)$$

(7)

FLUENT provides a solar load model that can be used to calculate radiation effects from the sun's rays that enter a computational domain. Two options were available for the model: solar ray tracing and discrete ordinates irradiation. The ray-tracing approach was a highly efficient and practical means of applying solar loads as heat sources in the energy equations. For optical thickness greater than 3 mm, the Rosseland model was cheaper and more efficient. In this case, the Rosseland Radiation Model with the solar loading and solar ray tracing was used [23]. This model allows calculating the intensity of incident solar radiation on a surface as well as the ambient temperature when the latitude and altitude of the application site were given.

3.4. Boundary Types and Conditions for the Model

Defining proper boundary types and boundary conditions were essential for accurate solution of a fluid flow problem. Most of the boundary conditions were determined by the physical phenomena but some were set by the simulation software. Table 1 shows the boundary types and boundary conditions for various parts of the geometric model.

The selection of boundary conditions was an important step in the CFD simulation. Any CFD tool solves the various equations involved in the modelling based on constraints put by the boundary conditions. The real or physical boundary conditions were idealized and simplified to put them in the simulation. For instance, in this study, the sidewalls of solar still that were physically insulated were considered to have the adiabatic wall boundary condition in the simulation setup.

Table 1: Boundary types and boundary conditions.

Zone Name	Zone Type	Thermal Conditions	Description	Wall Thickness, (m)
Glass Wall	Wall	Convection ($2\ W/m^2.k$)	Semi-Transpwerent	0.003
Acrylic Wall	Wall	Coupled	Semi-Transpwerent	0.004
Absorber Wall	Wall	Adiabatic (Heat flux = 0)	Opaque	0.0008
Front Wall	Wall	Adiabatic (Heat flux = 0)	Opaque	0.05
Back Wall	Wall	Adiabatic (Heat flux = 0)	Opaque	0.05
Side wall Right	Wall	Adiabatic (Heat flux = 0)	Opaque	0.05
Side wall Left	Wall	Adiabatic (Heat flux = 0)	Opaque	0.05

3.5. Selection of Models and Constants for Simulation:

The operating parameters and models used for simulation of multiphase SSDBSS of the FLUENT solver were given in Table 2.

Having fixed the input parameters, the solution was initialized. The time step for the iterations was set equal to 0.001-1.0 s depending on the ease of convergence and time required to complete the simulation.

Table 2: Input Parameters of the Solver

Function	Specification			
Solver Setting	Space	3-D		
	Time	Unsteady, 1st-Order Implicit		
	Viscous Model	RNG k-epsilon Turbulence Model with Enhanced Wall Treatment Thermal Effects And Viscous Heating		
	Multiphase Model	Volume of Fluid (VOF) Model	Implicit Scheme	
	Radiation	Rosseland Radiation Model, Solar Loading and Solar Ray Tracing Inputs: (latitude 30.5° N and longitude 31.01° E) Day: 14.06 Time: 07.00 AM Directions of the still Using Solar Calculator		
Material Properties	Solid	Glass, Acrylic, GI Sheet and Wood	Thermo-physical properties including density, thermal conductivity and specific heat capacity of the materials	τ_g: 0.96
	Fluid	Air, Water-Liquid and Water-Vapor		τ_w: 0.98
Phases	Three Phase	Primary Phase	Air	
		Secondary Phase	Water-Liquid	
			Water-Vapor	
Operating Conditions	Operating Pressure	1.01 Bar		
	Gravity	-9.81, Z-Direction		
	Operating Temperature	288.16 K		

4. Results and Discussion

The amount of water contained in the lower basin of the SSDBSS can be identified by the water depth in the basin. As for the upper basin, a new characteristic parameter was introduced in this work for describing the amount of saltwater to be distilled in this basin. This parameter was called the equivalent water depth and it was defined as the water depth of the amount of the saltwater contained in the upper basin of the SSDBSS if it was poured into the lower still basin of this still. Throughout the work conducted here half the amount of the saltwater was poured into the upper basin and the other half was held in the lower basin. Hence the water depth in the lower basin was equal to the equivalent water depth

Unsteady simulation of the SSDBSS was carried out for the 14th June from 07:00 AM to 20:00 PM at a water-/equivalent water depth of 2cm, which was equivalent to 20 lit. Figure 7 shows the global solar radiation intensity of simulated and measured data on 14th June. Referring to Fig. 7, the results indicated that there were similar trends and good agreement between the simulated results and measured data for the global solar radiation intensity all over the day (maximum discrepancy amounts to 12.7%). Also, it can be seen that the solar radiation was increased gradually with the local time and reached maximum values at noon according to the weather conditions and then it decreased for both the simulated and the experimental results.

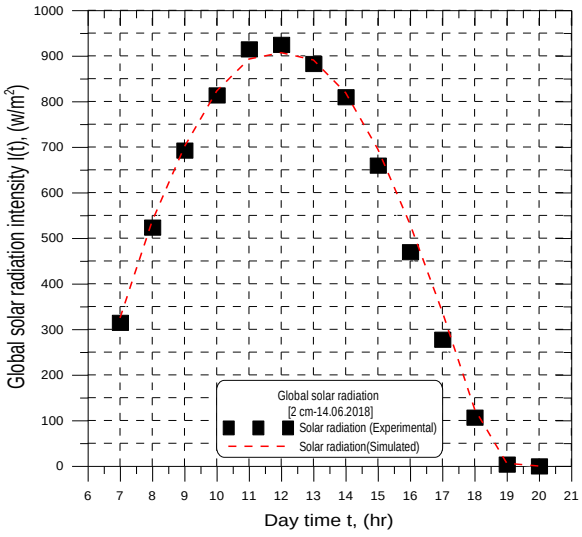

Fig. 7: Hourly variation of simulated and experimental solar radiation intensity on the 14th June.

In the solar still, the temperatures of the glass cover and the acrylic base, water in the basins, and the interior of the still play a vital role in the distillation of saltwater. In general, the amount of distillate produced by the solar still depends upon the temperature difference between water in the lower basin and condensing acrylic base of the upper basin, as well as the temperature difference between the water in the upper basin and condensing glass cover. The temperature contours of the absorber plate (base of the lower basin) for the tested SSDBSS at different time intervals with a water-/equivalent water depth of 2 cm were shown in Figure 8. The colour coding for temperatures in Kelvin was also shown on the charts. The "Blue" colour shows the minimum value of temperatures and the "Red" colour shows the maximum value of temperatures. The contours of the absorber plate temperature charts suggest that:

- Within the tested solar still configuration, the temperature of the absorber plate begins to rise as the solar radiation falls on the basin. The temperature contours show gradual rising increments till 14:00, and after that, they decrease steadily.

- The effect of the shadow of the sidewalls was very clear on the absorber plate. As the sun rises from North-East, the effect of the shadow of the right sidewall was seen in the right part on the absorber plate of the still, Figs. (8-a and 8-b), and during sunset at north-west, the effect of shadow of the left sidewall can be seen in the left part on the absorber plate of the still, Figs. (8-c and 8-d).

The temperature contours of the mixture (wet air) inside the SSDBSS at the X-Y plane passing through the still center and parallel to its sidewalls were drawn in Figure 9, at different time interval through the daytime were shown. It can be seen from Fig. 9 that:

- Within the tested SSDBSS model, the temperature of the water begins to rise as the solar radiation falls on the basins. After some time water gets heated up and evaporation takes place which results in the vapor formation in the still as well as increase in the interior temperatures. The contours of interior temperatures show the increment of an increase in the interior temperature of solar still with time.

- The interior temperature of the tested SSDBSS follows the pattern of solar radiation falling over the glass/acrylic covers. The interior temperatures of air and water vapor mixture inside the tested SSDBSS increase gradually up to 14:00 and after that, they decrease gradually.

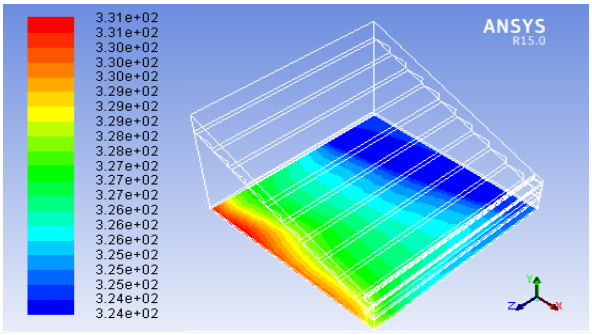

a) Temperature contour at10:00

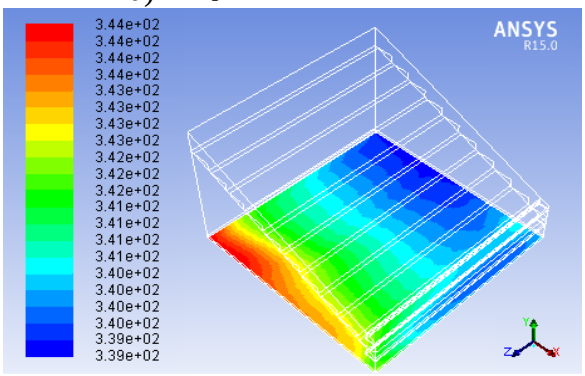

b) Temperature contour at 12:00

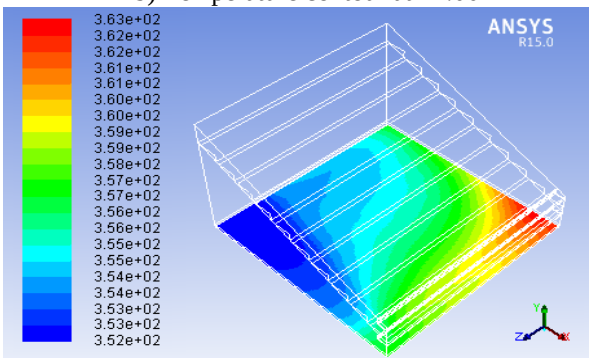

c) Temperature contour at 14:00

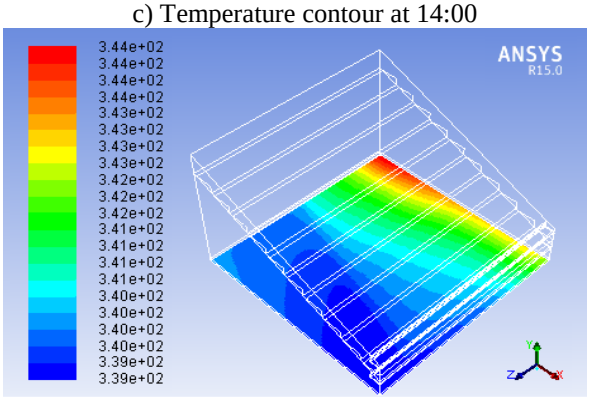

d) Temperature contour at 16:00

Fig. 8: Temperature contours of the absorber plate at different time intervals for the single slope, double basin solar still at a water-/equivalent water depth of 2cm.

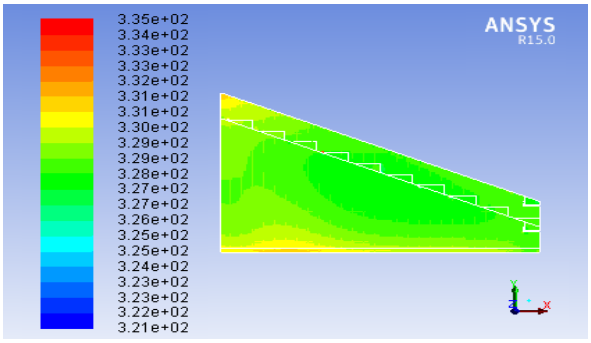

a) Temperature contour at 10:00

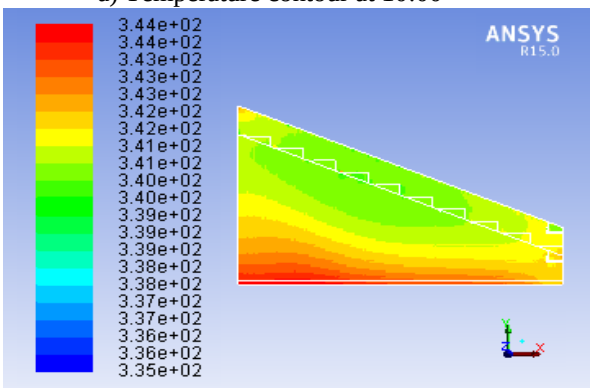

b) Temperature contour at 12:00

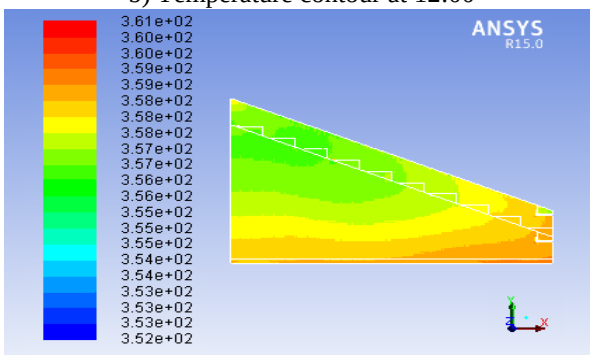

c) Temperature contour at 14:00

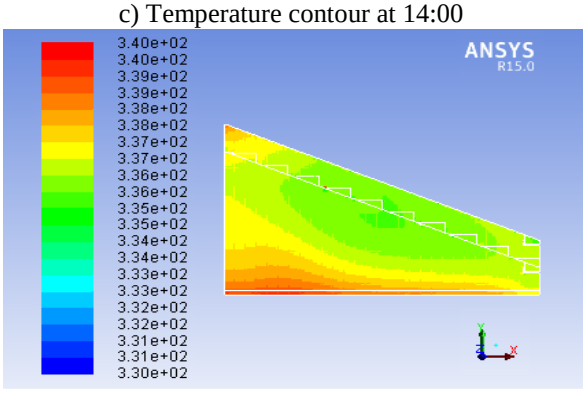

d) Temperature contour at 16:00

Fig. 9: Temperature contours of the inside mixture at the X-Y plane at different times for the single slope, double basin solar still at a water-/equivalent water depth of 2cm.

Figure 10 shows a comparison between the average simulated results and experimental results of the temperature of the saltwater, as well as the acrylic and glass covers for a water-/equivalent water depth of 2cm. According to Figure 10 (A and B), the results indicated that there were similar trends and good agreement between the simulated results and measured data for the water, and glass and acrylic cover temperatures all over the day (the maximum error was estimated to be 3.5%). The small deviation of the predicted and measured data was accounted for by the fact that FLUENT takes the ideal characteristics of water, glass, and acrylic covers and not the actual properties. Also, the most likely reason for this deviation was that the values of solar radiations taken in the simulation were higher than the measured values as suggested by Fig. 7.

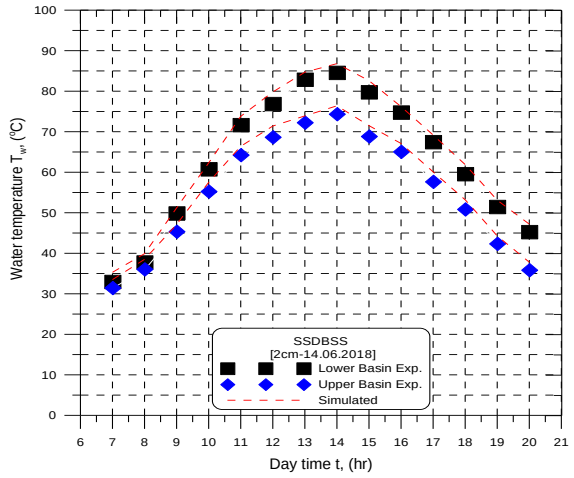

(A)

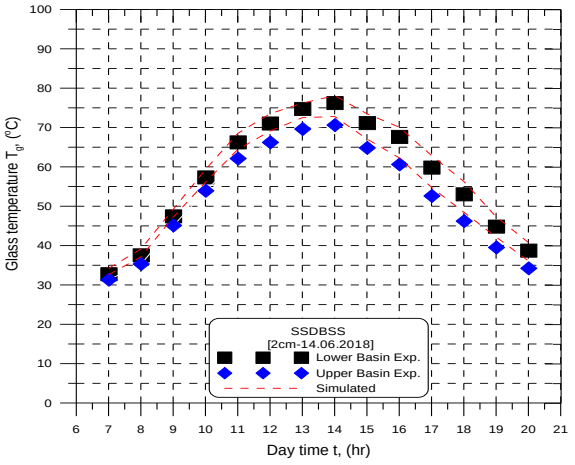

(B)

Fig. 10: Comparison between simulated and experimental results of water and glass cover temperatures for the studied solar still at a water-/equivalent water depth of 2cm.

Referring to Figure 10, it can be seen also that the temperatures of the saltwater and acrylic and glass covers increase from 07:00 to 14:00 monotonically for the tested solar still, and after 14:00 PM, they decrease monotonically too. This follows the trend of the intensity of solar radiation, as expected.

As the saltwater in the still basins gets heated by the incident solar radiation water was evaporated and the air above the water surfaces increases in relative humidity and becomes saturated. The warmer air flows upwards touching the cooler transparent surfaces where it gets cooled, and the water vapor contained in the air was partially condensed. As the temperatures inside the tested solar still rise with the time, the composition of mixture phases keeps on changing. Figure 11 illustrates the volume fraction of water vapor for the SSDBSS at different time intervals with a water-/equivalent water depth of 2cm. The color coding for the volume fraction of water vapor was also shown on the charts of Fig. 11. The "Blue" color shows the minimum value of volume fraction and the "Red" color stands for the maximum value of the volume fraction. The volume fraction range covers the complete domain. From the contour charts of the volume fraction of water vapor for the tested solar still configuration, it was observed that:

- As the temperature increases, the volume fraction of water vapor was magnified significantly.

- The volume fraction of the water vapor increases till 14:00 and thereafter it starts decreasing as the solar intensity recedes.

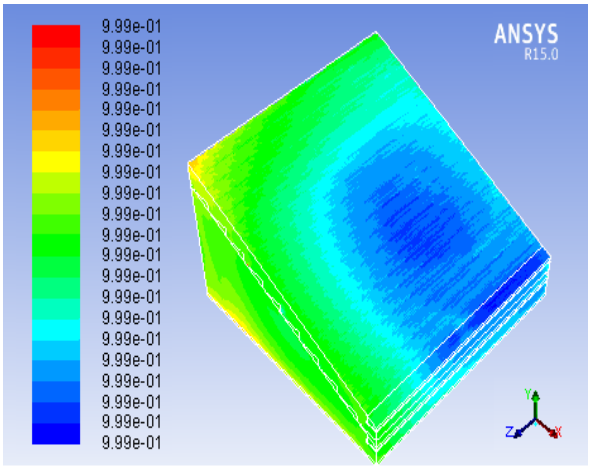

a) Water vapor contour at 10:00

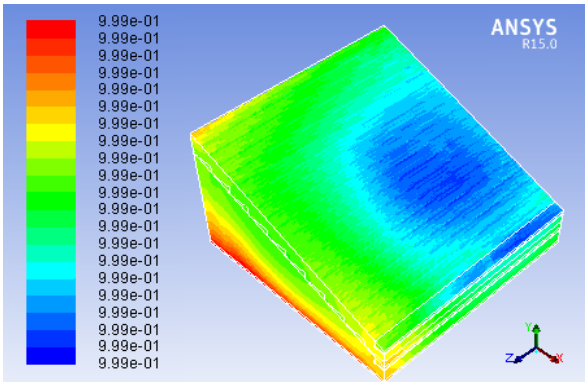

b) Water vapor contour at 12:00

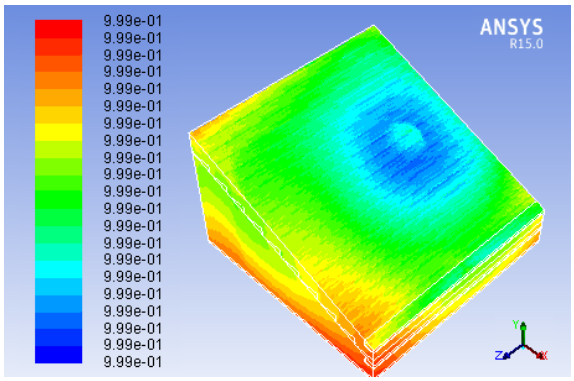

c) Water vapor contour at 14:00

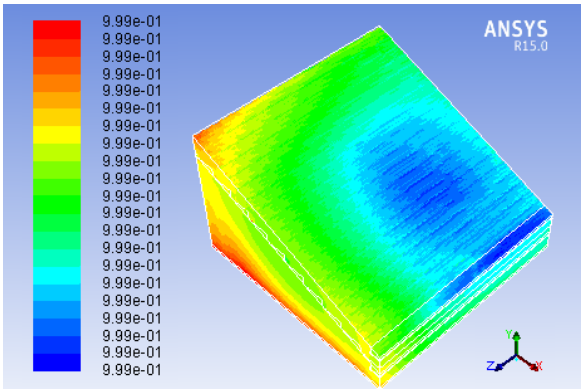

d) Water vapor contour at 16:00

Fig. 11: The contours of volume fraction of water vapor at different time intervals for the studied still at a water-/equivalent water depth of 2cm.

Figure 12 (A and B) shows a comparison of the hourly and accumulated productivities values, respectively, obtained experimentally and numerically for the tested SSDBSS and for a water-/equivalent water depth of 2cm. Fig.12 suggests that the daily simulated and experimental accumulated productivities of the examined SSDBSS were found to be 3.148 lit/m^2 and 2.855 lit/m^2. Moreover Fig. 12 indicates clearly that the pattern of experimental graphs was very close to the simulated ones, which shows a good agreement between the CFD prediction (simulated) and experimental values for the tested solar still (maximal discrepancy comes to 10.26 %).

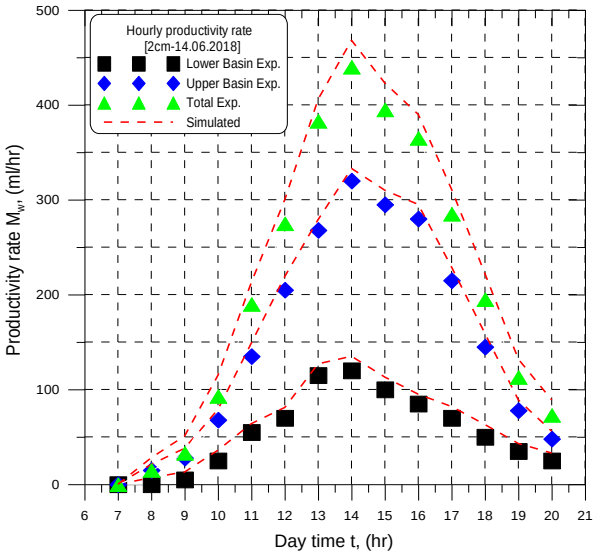

(A)

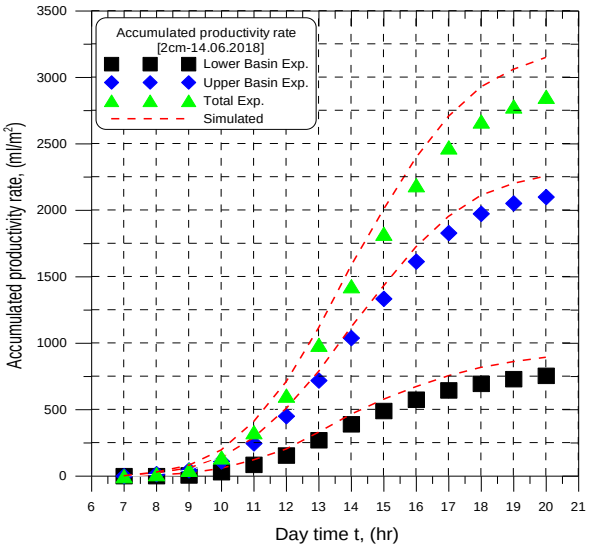

(B)

Fig. 12: Comparison between simulated and experimental results of hourly and accumulated productivities for the examined solar still at 2cm water-/equivalent water depth.

The solar still efficiency signifies the capability of the still in desalinating saltwater and can be practiced as a parameter that should be maximized for finding out the optimal still design. The ratio of the total amount of thermal energy used to get a certain amount of distillate output in a certain duration to the energy supplied to the solar still during the same duration was known as thermal distillation efficiency. Figure 13 illustrates the simulated and experimental daily

efficiency of the studied SSDBSS. The experimental value of daily efficiency was slightly less than the simulated value, which shows a fair agreement between simulated and experimental results with a maximum difference of 10.6%. Experimental efficiency was lower than the simulated one due to the possible leakage of vapor. Additionally, it was obvious from Fig. 13 that the daily experimental thermal efficiency of the SSDBSS was 25% for a water-/equivalent water depth of 2cm. Also, it's important to refer that the daily experimental thermal efficiency of the conventional single slope solar still was 15.5% for a water depth of 2cm and for the same dimensions and tested weather conditions [10].

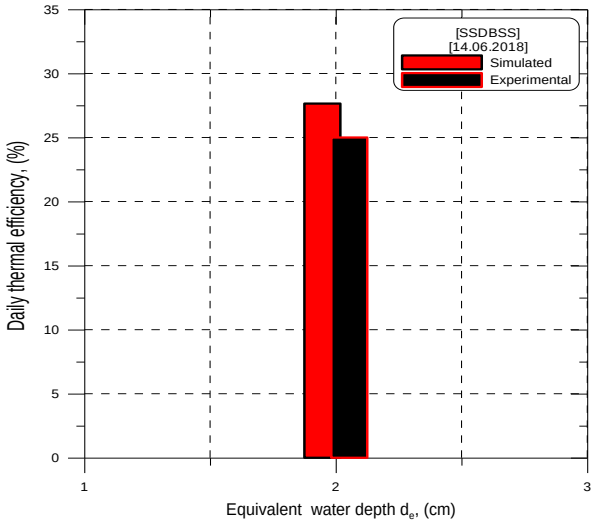

Fig. 13: Simulated and experimental daily efficiency for the studied solar still with a water-/equivalent water depth of 2cm.

5. Conclusions

The main objective of the current study was to design and manufacture a new configuration of basin type solar still, namely single slope double basin solar still SSDBSS, as well as to develop a 3-D CFD model to simulate the behavior of the proposed still configuration. The experimental and numerical results of the present research led to draw the following Conclusions:

1. CFD simulation was a powerful tool for design and parameter analysis of solar still. The simulation results were compared with the available experimental data of the SSDBSS. The simulation amount of solar intensity, freshwater productivity as well as water and condensing glass/acrylic covers temperatures were in good agreement with the experimental data.

2. The daily simulated and experimental accumulated productivities of the SSDBSS were found to be 3.148 lit/m^2 and 2.855 lit/m^2 for a water-/equivalent water depth of 2cm.

3. The simulated and experimental daily efficiency was around 27.65% and 25%, respectively for the SSDBSS for 2cm water-/equivalent water depth. The daily experimental thermal efficiency of the conventional single slope solar still was 15.5% at 2cm water depth for the same dimension and tested weather conditions.

Author Contributions: Mahmoud S. El-Sebaey: Designing and manufacturing the experimental setup, performing the CFD simulation and analyzing the results. Ahmed Hegazy: Analysis of the achieved data and preparing for the design of the experiments, analyzing the results, and contributing to the scientific discussion. Asko Ellman: Analysis of the achieved data, cooperating in the scientific discussion. Tarek Ghonim: English correction.

Nomenclature

Variable	Definition
A_b	Basin liner surface area of still m^2
C_w	Specific heat capacity of the water in the solar still (J/kg °C)
$\overline{F}$	The body force.
$\overline{g}$	The acceleration due to gravity.
G	The incident radiation.
K_{eff}	The effective conductivity.
n	The number of phases.
$\dot{q}_r$	Radiation heat transfer.
$\dot{q}_c$	Convection heat transfer.
$\dot{q}_{ev}$	Evaporation heat transfer.
S_E	Includes any other volumetric heat sources.
$\overline{v}_m$	The mass-averaged velocity.
$\overline{v}_{dr,k}$	The drift velocity for secondary phase k.

Greek symbols

α	Absorptivity
α_k	The volume fraction of phase k.
ρ_m	The mixture density.
τ	Transmissivity
μ_m	The viscosity of the mixture.

Abbreviations

SSDBSS	Single slope double basin solar still

6. References:

[1] UNICEF, USA, Water and Sanitation, [ONLINE]. [Cit. 15th November 2018]. https://www.unicefusa.org/mwassion/survival/water

[2] Pietro C., Andrea C., and Francesco G., 2018, Thermodynamic, Exergy, and Thermoeconomic analysis of Multiple Effect Distillation Processes", Renewable Energy Powered Desalination Handbook, pp.445-489.

[3] Tiwari G. N. and Sahota L., 2017, "Review on the energy and economic efficiencies of passive and active solar distillation systems", Desalination, Vol. 401, pp.151-179.

[4] Walton. J. Lu. H, Turner. Ch., Solis. S. and Hein. H, 2004 "Solar and waste heat desalination by membrane distillation", US Department of the Interior, Bureau of Reclamation, DWPR, No. 81.

[5] Yi-Ning Wang and Rong Wang, 2019, "Reverse Osmosis Membrane Separation Technology", Membrane Separation Principles and Applications, pp.1-45.

[6] Imad Al-Hayeka, Omar O. Badran, 2004, "The effect of using different designs of solar stills on water distillation", Desalination, Vol. 169, pp. 121- 127.

[7] Ahsan, A., Imteaz, M., Rahman, A., and Yusuf, B. 2012, "Design, fabrication and performance analysis of an improved solar still", Desalination, Vol. 292, pp.105–112.

[8] Elango T.and Murugavel K. K., 2015, "The effect of the water depth on the productivity for single and double basin double slope glass solar stills", Desalination, Vol.359, pp. 82-91.

[9] El-Sebaii A. A., 2005, "Thermal performance of a triple-basin solar still", Desalination, Vol. 147, pp. 23-37.

[10] Mahmoud S. El-Sebaey, A. Ellman, A. Hegazy and T. Ghonim, An Experimental Investigation on Productivity and Performance of an Improved Design of Basin Type Solar Still , 21th International Conference on Desalination and Renewable Energy (ICDRE 2019), Copenhagen, Denmark, 11-12 June (2019).

[11] Ahmed M. I., Hrairi M., and ismail A.F., 2009, "On the characteristics of multistage evacuated solar distillation", Renewable Energy, Vol. 34, pp. 1471- 1478.

[12] Vaibhav R. K., Abhay P. S., Hemant K. and Rahul K., 2017, "Modelling and Performance Enhancement of Single Slope Solar Still using CFD", Energy Procedia, Vol. 109, pp. 447- 455.

[13] Shakaib M. and Khan M. A., 2015, "Modeling of Fluid Flow and Temperature Profiles in Solar Stills Using CFD", Proceedings of 2015 International Conference on Chemical, Metallurgy and Environmental Engineering (ICMAEE-15), istanbul (Turkey), June 3-4, pp. 272-276

[14] Singh A. and Mittal M. K., 2014, "Simulation of single slope solar still at different inclinations using CFD", International Conference of Advance Research and Innovation (ICARI-2014).

[15] Rahbar N. and Esfahani J.A., 2013, "Productivity estimation of a single-slope solar still: Theoretical and numerical analysis", Energy, Vol. 49, pp, 289-297.

[16] Muhammad S. and Masood A. K., 2015, "Modeling of Fluid Flow and Temperature Profiles in Solar Stills Using CFD", International Conference on Chemical, Metallurgy and Environmental Engineering, pp. 272-276.

[17] Hitesh N. P. and Shah P. K., 2011, "Modelling and verification of single slope solar still using ANSYS CFX", International Journal of Energy and Environment, Vol. 2(6), pp. 985-998.

[18] Badusha A. R. and Arjunan T. V., 2011, "Performance analysis of single slope solar still", Desalination, Vol. 268, pp. 103-110.

[19] Setoodeh N., Rahimi R.., and Amer A., 2011, "Modeling and determination of heat transfer coefficient in a basin solar still using CFD", Desalination, Vol.268, pp. 103-110.

[20] Tiwari A. K. and Tiwari G. N., 2006, "Effect of water depths on heat and mass transfer in a passive solar still: in summer climatic condition", Desalination, Vol. 195, pp. 78-94.

[21] Badran O., Abu-khader M. M., 2007, "Evaluating thermal performance of a single slope solar still", Heat and Mass Transfer, Vol. 43, pp. 985-995.

[22] Vaibhav R. K., Abhay P. S., Hemant K. and Rahul K. 2017, "Modelling and Performance Enhancement of Single Slope Solar Still using CFD", Energy Procedia, Vol.109, pp. 447-455.

[23]https://www.afs.enea.it/project/neptunius/docs/fluent/html/th/node113.htm.